

# HIGHER-ORDER LEAST-SQUARES RECONSTRUCTION FOR TURBULENT AERODYNAMIC FLOWS

Alireza Jalali\* and Carl Ollivier-Gooch<sup>†</sup>

\* Department of Mechanical Engineering  
University of British Columbia  
2054-6250 Applied Science Lane, Vancouver, BC, V6T 1Z4, Canada  
e-mail: arjalali@interchange.ubc.ca

<sup>†</sup>Department of Mechanical Engineering  
University of British Columbia  
2054-6250 Applied Science Lane, Vancouver, BC, V6T 1Z4, Canada  
e-mail: cfog@mech.ubc.ca

**Key words:** Reconstruction, Least-squares, Anisotropic, Finite Volume, Turbulent

**Abstract.** It is well understood that the cell-centered least-squares reconstruction suffers from poor accuracy for high aspect ratio meshes with curvature. Since these meshes are required for turbulent simulations, a sufficiently accurate reconstruction of primitive variables are required. In this paper, we present a new method for higher-order solution reconstruction on high aspect ratio curved meshes that resolves the accuracy issues.

## 1 INTRODUCTION

Higher order — higher than second order — computation of fluid dynamic equations is a demanding issue, motivated by a potentially significant cost reduction for complex CFD problems. For structured meshes, using a higher-order accurate method can be more efficient both in terms of solution time and memory usage [1]. Research in high-order unstructured solvers is motivated by the accuracy and efficiency advantages proved in the application of these schemes on structured meshes with the flexibility of unstructured meshes for complex geometries.

A key point in the development of higher-order methods for unstructured meshes is a higher-order reconstruction of primitive variables within the control volumes. The construction of a  $k$ -exact reconstruction operator is one way to reconstruct a solution polynomial based on the control volume data. This method dates back to Barth and Frederickson's work designing a quadratic reconstruction operator to estimate the advective flux of the Euler equations [2]. Later, Ollivier-Gooch and Van Altena [3] employed a  $k$ -exact reconstruction procedure for advection-diffusion problems.

In the context of turbulent flows for aerodynamic applications, it is quite common to have cells whose aspect ratios are about 10,000. Furthermore, aerodynamic configurations typically consist of curved surfaces on which a flow boundary layer develops. As a result, the simulation of high Reynolds number turbulent flows requires sufficiently accurate polynomial approximation on high aspect ratio meshes with finite curvature. Mavriplis [4] examined the accuracy of the least-square technique for second-order discretization on unstructured meshes. For a cell-centered method on triangular meshes with high curvature, he showed that the computed cell gradient exhibits poor accuracy even after weighting the least-squares system to emphasize geometrically close data.

In this paper, we will investigate the accuracy of high-order solution reconstruction on highly anisotropic meshes with finite curvature for cell-centered discretizations. Our numerical results show that the cell-centered least-squares reconstruction in its traditional fashion degrades the solution accuracy on high aspect ratio curved meshes and adding a weight function does not resolve the issue. Consequently, a new least-squares reconstruction framework is proposed in which a local tangential-normal coordinate system is obtained by solving an auxiliary LS problem. We will show that the new coordinate system improves the accuracy significantly for high aspect ratio cells with curvature.

## 2 LEAST-SQUARES RECONSTRUCTION

The flow solver approximates the unknown variables of the flow field,  $u$ , in the control volume by reconstructing a piecewise polynomial about the control volume's reference point  $(x_i, y_i)$ .

$$u_i^R(x, y) = u|_i + \frac{\partial u}{\partial x}\Big|_i (x - x_i) + \frac{\partial u}{\partial y}\Big|_i (y - y_i) + \frac{\partial^2 u}{\partial x^2}\Big|_i \frac{(x - x_i)^2}{2} + \dots \quad (1)$$

In Equation 1,  $u_i$  is the value of the reconstructed solution and  $\frac{\partial^{k+l} u_i}{\partial x^k \partial y^l}$  are its derivatives at the reference point of control volume  $i$  which is its centroid for cell-centered schemes.

The flow solver uses a least-squares reconstruction method to determine the coefficients of the Taylor polynomial. In this method, the coefficients are computed by conserving the mean value in the control volume and minimizing the error in predicting the mean value of nearby control volumes [3]. The conservation of the mean within a control volume requires that

$$\bar{u}_i = u|_i + \frac{\partial u}{\partial x}\Big|_i \bar{x}_i + \frac{\partial u}{\partial y}\Big|_i \bar{y}_i + \frac{\partial^2 u}{\partial x^2}\Big|_i \frac{\bar{x}_i^2}{2} + \dots \quad (2)$$

where  $\bar{x}^n \bar{y}^m$  are the moments of area about the reference location. In addition, the error of the mean value of the reconstructed solution for control volumes in the stencil  $\{V_j\}_i$  should be minimized. The mean value for a single control volume  $V_j$  of the reconstructed solution  $u_i^R$  is

$$\bar{u}_j = u|_i + \frac{\partial u}{\partial x}\Big|_i \hat{x}_{ij} + \frac{\partial u}{\partial y}\Big|_i \hat{y}_{ij} + \frac{\partial^2 u}{\partial x^2}\Big|_i \frac{\hat{x}_{ij}^2}{2} + \dots \quad (3)$$

where  $\widehat{x^n y^m}_{ij}$  are the moments of control volume  $j$  about the centroid of control volume  $i$ . This equation is written for every control volume within the stencil of control volume  $i$ . The minimum number of control volumes in the stencil is more than what is required (3, 9 and 15 for second-, third- and fourth-order reconstruction, respectively). The resulting least-squares problem is

$$\begin{bmatrix}
 1 & \bar{x}_i & \bar{y}_i & \bar{x}^2_i & \bar{xy}_i & \bar{y}^2_i & \cdots \\
 \hline
 w_{i1} & w_{i1}\widehat{x}_{i1} & w_{i1}\widehat{y}_{i1} & w_{i1}\widehat{x^2}_{i1} & w_{i1}\widehat{xy}_{i1} & w_{i1}\widehat{y^2}_{i1} & \cdots \\
 w_{i2} & w_{i2}\widehat{x}_{i2} & w_{i2}\widehat{y}_{i2} & w_{i2}\widehat{x^2}_{i2} & w_{i2}\widehat{xy}_{i2} & w_{i2}\widehat{y^2}_{i2} & \cdots \\
 w_{i3} & w_{i3}\widehat{x}_{i3} & w_{i3}\widehat{y}_{i3} & w_{i3}\widehat{x^2}_{i3} & w_{i3}\widehat{xy}_{i3} & w_{i3}\widehat{y^2}_{i3} & \cdots \\
 \vdots & \vdots & \vdots & \vdots & \vdots & \vdots & \ddots \\
 w_{iN} & w_{iN}\widehat{x}_{iN} & w_{iN}\widehat{y}_{iN} & w_{iN}\widehat{x^2}_{iN} & w_{iN}\widehat{xy}_{iN} & w_{iN}\widehat{y^2}_{iN} & \cdots
 \end{bmatrix}
 \begin{pmatrix}
 u \\
 \frac{\partial u}{\partial x} \\
 \frac{\partial u}{\partial y} \\
 \frac{1}{2} \frac{\partial^2 u}{\partial x^2} \\
 \frac{\partial^2 u}{\partial x \partial y} \\
 \frac{1}{2} \frac{\partial^2 u}{\partial y^2} \\
 \vdots
 \end{pmatrix}_i = \begin{pmatrix}
 \bar{u}_i \\
 w_{i1}\bar{u}_1 \\
 w_{i2}\bar{u}_2 \\
 w_{i3}\bar{u}_3 \\
 \vdots \\
 w_{iN}\bar{u}_N
 \end{pmatrix} \tag{4}$$

where the line separates the conservation of mean constraint from equations to be solved by least-squares. In this problem, inverse-distance weights,  $w_{ij}$ , can be set to emphasize the importance of nearby data.

### 3 METHODOLOGY

#### 3.1 Interior Curving Strategy

For second-order accurate solvers, the surface of the curved geometry is often represented by a series of linear elements that are not adequate for higher-order accuracy. As a result, the effect of curvature must be taken into account in higher-order solvers by a more accurate representation of boundary faces. When the mesh is comprised of isotropic triangles, it is possible to just deform the boundary of the elements which are in contact with the curved boundary. However, this strategy fails when the triangles are highly anisotropic as is common in boundary layer regions. In this situation, it is necessary to propagate the mesh deformation into the domain interior to prevent faces from intersecting near curved boundaries. To curve the interior faces of a mesh, there are different suggestions in literature [5, 6]. In this paper, we use a modified linear elasticity method due to Wang *et al.* [7] to project the boundary curvature into the interior edges. In this method, the deformations are represented using continuous piecewise polynomials within each element of the original unstructured mesh. For this purpose, six-node quadratic and ten-node cubic triangular elements are used to represent the boundary geometry up to third- and fourth-order accuracy, respectively. On the boundary of the domain, the displacement vectors are known and thus Dirichlet boundary conditions are imposed. Solving the linear elasticity problem gives the displacement, and thus the location of nodes in the curved mesh.

As described in Section 2, the least-squares solution reconstruction requires the moments of each control volume about its reference point (Equation 2). These moments can

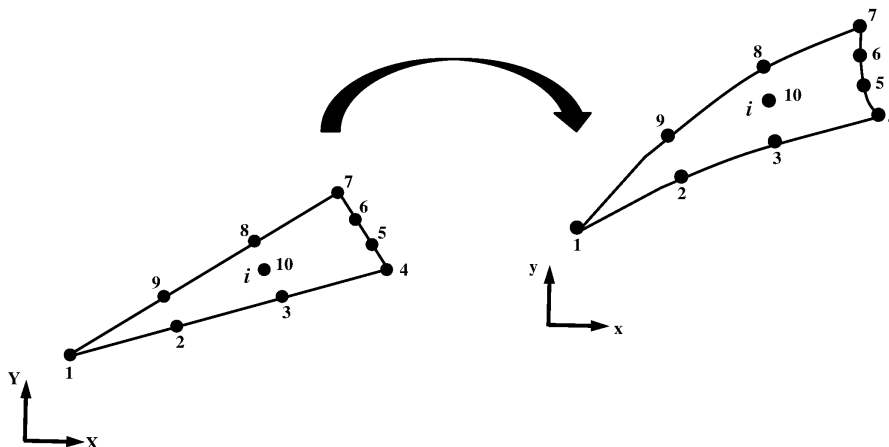


Figure 1: The mapping from the reference triangle to the curved element

be easily computed for a linear element by the use of Gauss quadrature integration rule for triangles; however, calculating the moments of area is not trivial for a curved element. Considering that the solution of the linear elasticity equation gives the location of all nodes of an element, the Cartesian coordinate of an arbitrary point within the reference triangle can be given using the finite element interpolation functions,  $\phi_j(X, Y)$ :

$$x(X, Y) = \sum_{j=1}^N x_j \phi_j(X, Y), \quad y(X, Y) = \sum_{j=1}^N y_j \phi_j(X, Y) \quad (5)$$

where  $N = 6$  for quadratic and 10 for cubic triangles. Figure 1 depicts the mapping from the straight reference triangle into the physical curved triangle for cubic elements. The reference point of the curved elements are set to be the mapped location of the reference triangles' centroid. For quadratic triangles, the Lagrange interpolation functions are equal to  $\phi_{1,3,5}^c = -1/9$  and  $\phi_{2,4,6}^c = 4/9$  for the centroid whereas the tenth node is coincident with the centroid for a cubic triangle and thus  $\phi_{10}^c = 1$ ,  $\phi_{1,\dots,9}^c = 0$ . Therefore,

$$x - x_i = \sum_{j=1}^N x_j (\phi_j - \phi_j^c), \quad y - y_i = \sum_{j=1}^N y_j (\phi_j - \phi_j^c)$$

We evaluate the moments of area for the physical curved element in  $(x, y)$  by integrating over the reference triangle in  $(X, Y)$  coordinate system:

$$\overline{x^n y^m}_i = \frac{1}{A_i} \int_{V_i} (x - x_i)^n (y - y_i)^m |J| dX dY \quad (6)$$

where  $J$  is the determinant of the Jacobian matrix:

$$J = \begin{vmatrix} \frac{\partial x}{\partial X} & \frac{\partial x}{\partial Y} \\ \frac{\partial y}{\partial X} & \frac{\partial y}{\partial Y} \end{vmatrix} \quad (7)$$

The integral over the reference triangle can be evaluated by using a sixth-order Gauss quadrature rule with seven quadrature points over straight triangles with the area of  $A_0$  to ensure that the numerical integration does not degrade the overall accuracy of the reconstruction:

$$\overline{x^n y^m}_i = \frac{1}{A_i} \sum_{g=1}^7 w_g (x(X_g, Y_g) - x_i)^m (y(X_g, Y_g) - y_i)^n |J_g| A_0 \quad (8)$$

### 3.2 Curvilinear Coordinate

As mentioned earlier, the simulation of high Reynolds number turbulent flows requires sufficiently accurate polynomial approximation on high aspect ratio meshes with finite curvature. It is well understood that the cell-centered  $k$ -exact LS reconstruction suffers from poor accuracy on highly skewed meshes over curved surfaces for second-order. Our numerical results in Section 4 yields the same conclusion for higher than second-order reconstruction even after weighting the least-squares system by geometrically close data.

Instead, we construct a local curvilinear coordinate system at the reference point of each control volume. For this purpose, we define a mapping from the physical space into a tangential-normal coordinate system for cells with high curvature near the walls:

$$\begin{aligned} t &= a_1(x - x_i) + a_2(y - y_i) + a_3(x - x_i)^2 + a_4(x - x_i)(y - y_i) + \dots \\ n &= b_1(x - x_i) + b_2(y - y_i) + b_3(x - x_i)^2 + b_4(x - x_i)(y - y_i) + \dots \end{aligned} \quad (9)$$

A quadratic mapping from  $(x, y)$  to  $(t, n)$  is sufficient for reconstruction up to third-order, whereas fourth-order reconstruction requires a cubic mapping. The mapping is obtained by the distance function and constructed tangential direction at the cell's reference points. The difference in distance from the wall determines the normal coordinate while the tangent coordinate is obtained by the projection of the vector connecting two reference points on the constructed tangential direction. This tangential direction is defined as the perpendicular direction to the normal to the wall direction as seen in Figure 2. The two sides of Equation 9 are evaluated for the same handful of control volumes used in the reconstruction stencil of a particular control volume. To find the mapping coefficients, an auxiliary least-squares system is solved to give the values of  $a_i$  and  $b_i$ .

For solution reconstruction in the new curvilinear coordinates, we require the moments of control volume  $i$  about its reference point:

$$\overline{t^n n^m}_i = \frac{1}{A_i} \int_{V_i} t^n n^m dA \quad (10)$$

The integration is performed over the curved triangles as described in Section 3.1 and the sixth-order quadrature rule is re-used to find the moments. For this purpose, the location of each Gauss point in the physical space  $(x_g, y_g)$  is obtained by Equation 5 and the corresponding Jacobian,  $J_g$ , is computed by Equation 7. Then, the non-linear mapping

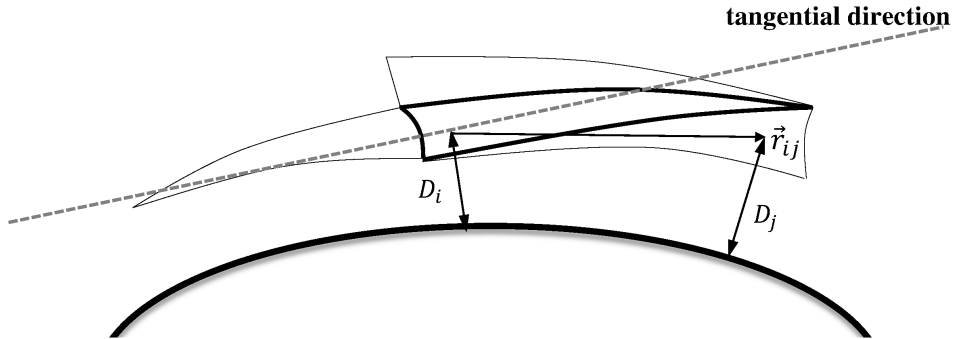


Figure 2: Illustration of tangential-normal coordinate construction

of Equation 9 is employed to find  $(t_g, n_g)$ . So the moment in the new coordinate system can be approximated by:

$$\overline{t^n n^m}_i = \frac{1}{A_i} \sum_{g=1}^7 w_g t_g^m n_g^n |J_g| A_0 \quad (11)$$

This procedure can be extended to compute the moments of control volume  $j$  about the reference point of control volume  $i$ , i.e.  $\widehat{t^n n^m}_{ij}$ . For these moments, the quadrature points of control volume  $j$  must be combined with the curvilinear mapping coefficients of control volume  $i$ .

## 4 RESULTS

In this section, we present the accuracy results of  $k$ -exact least-squares reconstruction on anisotropic meshes over curved surfaces. For this purpose, we first generate anisotropic triangular meshes over a circular arc and use a boundary layer type function to reconstruct. The reconstruction procedure both in its traditional form and on the new curvilinear coordinate system is performed and the results are compared. Then, we extend the analysis to more general meshes by testing in the anisotropic boundary layer region of unstructured triangular meshes over the NACA 0012 airfoil.

### 4.1 Circular Arc

Considering that anisotropic meshes are used to capture solution anisotropy, an anisotropic function must be manufactured to be employed in reconstruction tests. One of the obvious candidates for such a function is the turbulent boundary layer velocity profile. In

this paper, we make use of Reichardt's [8] empirical boundary layer profile:

$$u = \left\{ 2.5 \ln(1 + 0.4y^+) + 7.8 \left( 1 - \exp\left(\frac{-y^+}{11}\right) - \frac{y^+}{11} \exp(-0.33y^+) \right) \right\} u^* \quad (12)$$

where  $y^+$  is the non-dimensional distance from the wall and  $u^*$  is the friction velocity:

$$y^+ = \frac{yu^*}{\nu}, \quad u^* = \sqrt{\frac{\tau_w}{\rho}} \quad (13)$$

In Equation 13,  $\tau_w$  is the wall shear stress which can be related to the friction factor

$$c_{f,x} = \frac{\tau_w}{\frac{1}{2}\rho U_\infty^2} \quad (14)$$

and approximated by the one-seventh law:

$$c_{f,x} = \frac{0.027}{(Re_x)^{1/7}}, \quad Re_x = \frac{U_\infty x}{\nu} \quad (15)$$

Using Equations 13 to 15, it is possible to simplify  $u^*$  and  $y^+$  :

$$u^* = \sqrt{\frac{0.0135}{(Re_L \bar{x})^{1/7}}}, \quad y^+ = \bar{y} \cdot Re_L \cdot \sqrt{\frac{0.0135}{(Re_L \bar{x})^{1/7}}} \quad (16)$$

where  $\bar{x}$  and  $\bar{y}$  are the non-dimensional coordinates based on the length of plate,  $L$ . We assume that  $L = 1$  and take  $Re_L = 10^7$  to provide highly anisotropic behavior for  $\bar{u} = u/U_\infty$ .

Since we are interested in anisotropic meshes over a circular arc, we replace  $y$  with distance from the wall in all above equations. Moreover,  $x$  is replaced with the horizontal distance from the leading edge. Recognizing that the manufactured solution of Equation 12 is singular at the leading edge, a  $40^\circ$  circular arc is considered whose initial edge is sufficiently away from the leading edge,  $\theta = -\pi/2$  (Figure 3). The grid is generated by  $(N + 1) \times (2N + 1)$  nodes which are uniformly distributed along the arc but stretched out the wall with a factor of  $s$ . The thickness of the first layer is set such that one control volume exists in the viscous sublayer ( $y^+ < 5$ ) for the coarsest mesh; this is shrunk by a factor of two at each level of refinement. The quadrilaterals formed by these nodes can be uniformly (uniform stencil) or randomly (random stencil) divided into two triangles and perturbed in both directions based on local radial spacing. We consider three different mesh sizes in which  $N = 8, 16, 32$  and  $s = 1.6, 1.25, 1.12$ , respectively. It is worth mentioning that for all these meshes, the maximum aspect ratio is about 6300. Figure 3 shows the anisotropic solution on a randomly triangulated mesh where  $N = 16$ .

Figure 4 shows the  $L_2$  norm of higher-order solution reconstruction error for the manufactured function of Figure 3 and the three meshes described. It is seen that the asymptotic order of error in the unweighted LS is not consistent with the order of reconstruction

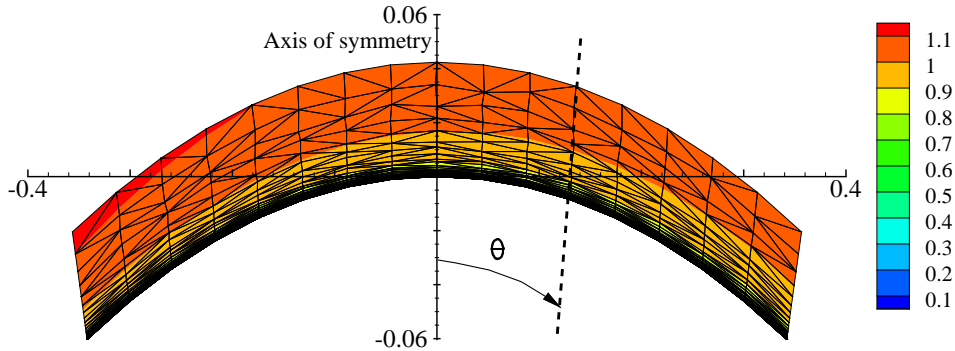


Figure 3: Anisotropic boundary layer type solution on a circular arc

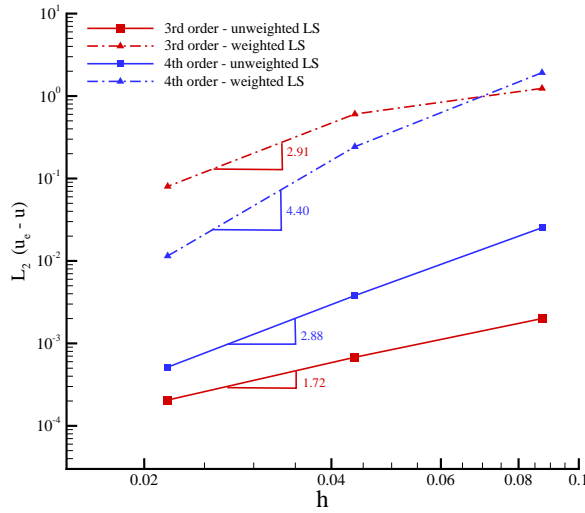
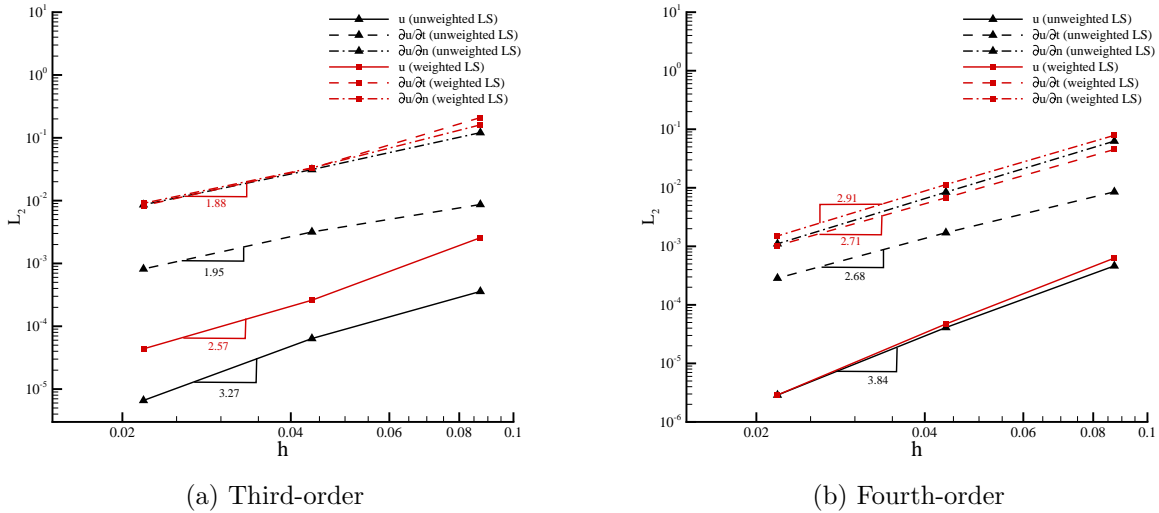


Figure 4: Reconstruction error using Cartesian coordinate system

in the range of mesh sizes considered here. Weighting the least-squares system corrects the asymptotic order of error but at the same time is associated with a noticeable increase in the value of error. The comparison of error values with the solution magnitude illustrated in Figure 3 implies a large relative error which is not acceptable. Therefore, traditional higher-order least-squares reconstruction suffers from accuracy issues for anisotropic meshes over curved surfaces regardless of the weight function.

On the other hand, the asymptotic order of reconstruction error using the new curvilinear coordinate system is consistent with the order of reconstruction and the error values are significantly smaller compared to the Cartesian coordinates. Figure 5 shows the reconstruction error for third- and fourth-order reconstruction in the tangential-normal coordinate system. Also, the first derivatives in both directions are one order less accurate than the solution, as expected. Note that the normal derivatives are larger due to the

Figure 5: Reconstruction error using curvilinear  $t - n$  coordinate system

No.	Number of grid points	Number of triangles	$N_s$	$h$	$AR_{max}$
1	$113 \times 33$	7168	65	0.031250	1552.91
2	$225 \times 65$	28672	129	0.015625	2442.76
3	$449 \times 129$	114688	257	0.0078125	3711.69

Table 1: NACA 0012 mesh specifications

anisotropic property of the test function and thus their relative errors are reported to be comparable with the tangential derivatives. Moreover, the use of an inverse-distance weighting reduces the accuracy of higher-order reconstruction as is clear in this figure.

## 4.2 NACA 0012

As a more general case for anisotropic triangular meshes over curved surfaces, we use the structured grids generated for turbulent RANS simulation by NASA Langley Research Center [9]. We randomly triangulate the quadrilaterals and curve the interior faces of the mesh to fourth-order using a cubic spline representation of the airfoil surface. Table 1 summarizes the specifications of the three meshes employed in this section for error analysis. In this table,  $N_s$  gives the number of points on the airfoil surface (both the lower and upper surfaces) distributed between the two edges ( $0 < x < 1$ ) and the mesh size is considered as the average horizontal distance between these points.

The meshes typically used for viscous flow simulations are comprised of different regions: anisotropic cells with curvature (R1), anisotropic straight cells (R2) and isotropic cells (R3). Since the calculation of mapping coefficients and moments of area are computationally more expensive for the curvilinear coordinate system, we need to isolate the

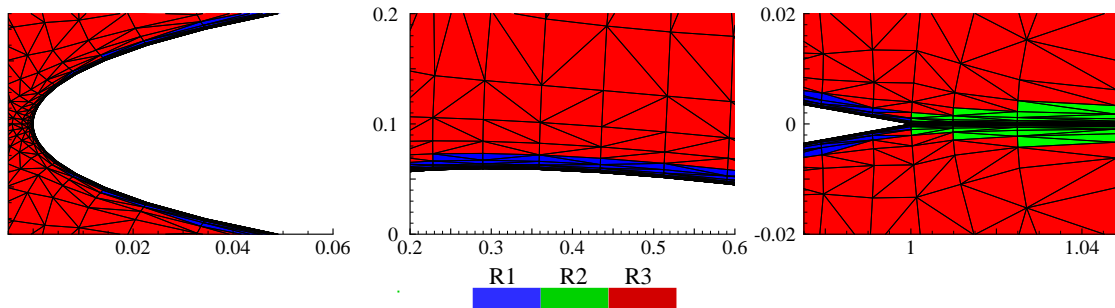


Figure 6: Separate regions for NACA 0012 meshes

regions that require this treatment. Our previous study shows that the LS reconstruction is well-conditioned and accurate for anisotropic straight meshes along their principal axes [10]. The anisotropic curved triangles can be recognized as those that have a large aspect ratio ( $AR > 10$  here) and are fairly well aligned with a wall. The latter can be understood by the angle between the line that connects the reference location to the closest point on the wall and the principal axis around which the second moment of area is minimum ( $\gamma < 10^\circ$ ). Figure 6 shows the separation of regions.

For reconstruction tests, we just consider R1 colored by blue because that is the region where traditional LS suffers from accuracy. An anisotropic solution should be manufactured for this region and some layers of neighbors in other regions. Therefore, we re-employ the boundary layer profile of Equation 12 for the triangles with a reference location in  $-0.1 < y < 0.1$  and  $x > -0.15$  and initialize other control volume averages with zero. In Equation 16,  $\bar{y}$  is replaced with  $D$  for the cells near the wall with a reference location in  $0 < x < 1$  and  $\bar{x}$  is replaced with  $x + 0.2$  to prevent singularities near the leading edge.

Figure 7 compares the  $L_2$ -norm of error in the reconstructed solution at the cells' reference locations between the Cartesian and curvilinear coordinate system for the triangles in R1. Similar to the results shown for the circular arc, the asymptotic order of error for unweighted LS in the Cartesian coordinate system is less than what was expected and weighting the LS system increases the error values. Contrarily, the curvilinear coordinate system yields error values that are significantly smaller and fall within the expected order. Again, the unweighted LS produces more accurate reconstructed solution.

## 5 CONCLUSION

The higher-order cell-centered finite volume solution reconstruction procedure was revisited on highly anisotropic meshes over curved surfaces to address the accuracy issues previously demonstrated for second-order. We performed our numerical tests on stretched triangular meshes with random stencil over a circular arc and also on meshes used for turbulent simulations over NACA 0012 airfoils. In both cases, we made up a boundary-layer

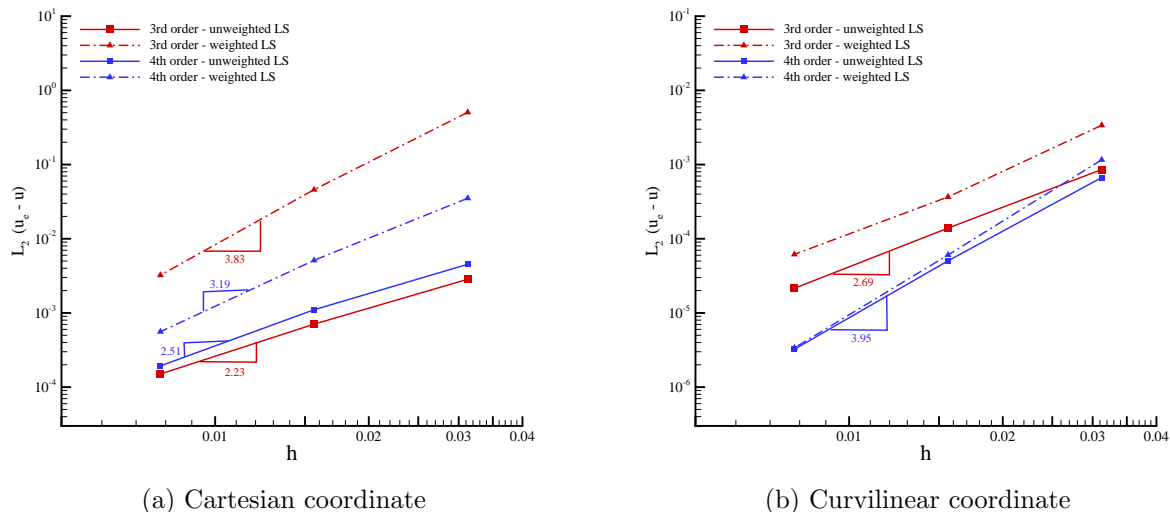


Figure 7: Solution reconstruction error for anisotropic curved region of NACA 0012

type anisotropic function for reconstruction.

Our results showed that the LS reconstruction in its traditional form leads to poor accuracy of approximated coefficients. Instead, we proposed a new method where a curvilinear coordinate system aligned with wall is constructed and used for reconstruction. The accuracy results in the proposed coordinates have small values of error and comply with the expected order of reconstruction with or without geometric weights. Nevertheless, the unweighted LS errors are noticeably smaller and thus outperform the weighted LS method.

## REFERENCES

- [1] S. De Rango and D. W. Zingg. Higher-order spatial discretization for turbulent aerodynamic computations. *American Institute of Aeronautics and Astronautics Journal*, 39(7):1296–1304, July 2001.
- [2] Timothy J. Barth and Paul O. Frederickson. Higher order solution of the Euler equations on unstructured grids using quadratic reconstruction. AIAA paper 90-0013, January 1990.
- [3] Carl F. Ollivier-Gooch and Michael Van Altena. A high-order accurate unstructured mesh finite-volume scheme for the advection-diffusion equation. *Journal of Computational Physics*, 181(2):729–752, 2002.
- [4] D. J. Mavriplis. Revisiting the least-squares procedure for gradient reconstruction on unstructured meshes. In *Proceedings of the Sixteenth AIAA Computational Fluid Dynamics Conference*, 2003.

- [5] S. J. Sherwin and J. Peiro. Mesh generation in curvilinear domains using high-order elements. *International Journal for Numerical Methods in Engineering*, 52(2-3):207–223, 2002.
- [6] P. O. Persson and J. Peraire. Curved mesh generation and mesh refinement using Lagrangian solid mechanics. In *Proceedings of the Forty-Seventh AIAA Aerospace Sciences Meeting*, 2009. AIAA 2009-949.
- [7] Li Wang, W. Kyle Anderson, J. Taylor Erwin, and Sagar Kapadia. Solutions of high-order methods for three-dimensional compressible viscous flows. In *Proceedings of the Twentieth AIAA Computational Fluid Dynamics Conference*, 2012.
- [8] H. Reichardt. Vollständige darstellung der turbulenten geschwindigkeitsverteilung in glatten leitungen. *ZAMM - Journal of Applied Mathematics and Mechanics / Zeitschrift für Angewandte Mathematik und Mechanik*, 31:208–219, 1951.
- [9] NASA Langley Research Center, Turbulence Modeling Resource. <http://turbmodels.larc.nasa.gov/>.
- [10] Alireza Jalali and Carl Ollivier-Gooch. Higher-order finite volume solution reconstruction on highly anisotropic meshes. In *Proceedings of the Twenty-First AIAA Computational Fluid Dynamics Conference*, 2013.